Petroleum Science 23 (2026) 5462–5473

Contents lists available at ScienceDirect

Petroleum Science

journal homepage: www.keaipublishing.com/en/journals/petroleum-science

Original Paper

Closed-loop internal multiple elimination

Zi-Lin He [a,b,c], Zhi-Na Li [a,b,*], Zhen-Chun Li [a,b], Yi-Peng Xu [c], Yan-Yun Leng [d]

[a] State Key Laboratory of Deep Oil and Gas, China University of Petroleum (East China), Qingdao, 266580, Shandong, China
[b] School of Geosciences, China University of Petroleum (East China), Qingdao, 266580, Shandong, China
[c] Shengli Geophysical Research Institute of Sinopec, Dongying, 257022, Shandong, China
[d] Shengli Oilfield Shengguang Technology Development Co., Ltd., Dongying, 257022, Shangdong, China

ARTICLE INFO

Article history:
Received 29 September 2025
Received in revised form
3 February 2026
Accepted 20 April 2026
Available online 24 April 2026

Edited by Meng-Jiao Zhou

Keywords:
Internal multiple suppression
Feedback model
IME
CL-IME

ABSTRACT

Internal multiple suppression is a crucial and challenging task in seismic data processing, aiming to mitigate the impact of internal multiples on imaging and seismic interpretation. A major difficulty arises because internal multiples often overlap with primaries, particularly in complex geological settings, making their accurate suppression difficult. Conventional internal multiple elimination (IME) methods rely on adaptive subtraction, which may cause primary energy loss in regions where primaries and internal multiples overlap. To address this issue, this paper derives internal multiple suppression formulas based on the well-known feedback model from a novel perspective. On this basis, we propose a Closed-Loop Internal Multiple Elimination (CL-IME) method. By formulating a new objective function, the proposed CL-IME method accurately estimates and suppresses internal multiples through inversion, thereby avoiding the primary energy loss associated with adaptive subtraction. Numerical experiments demonstrate that CL-IME achieves significantly higher accuracy than conventional IME in suppressing internal multiples, particularly in regions where primaries and multiples strongly overlap, thereby providing a more reliable approach for seismic data processing in complex structural settings.

1. Introduction

In seismic exploration data processing, internal multiples are challenging to identify and separate in seismic records due to their complex propagation paths, strong kinematic similarity to primaries, and significant temporal and spatial overlap with primaries. Their presence not only severely degrades the signal-to-noise ratio of seismic sections but can also result in misinterpretation of subsurface structures (Gong et al., 2017). Therefore, high-precision suppression of internal multiples is not only essential for enhancing seismic imaging quality but also represents a significant scientific challenge in geophysical exploration (Li et al., 2024). Currently, a widely used approach for internal multiple suppression is the Internal Multiple Elimination (IME) method (Jakubowicz, 1998), which serves as the theoretical foundation for our proposed method. Another relatively high-precision method is the Inverse Scattering Series (ISS) approach (Araújo et al., 1994; Yang and Zhu, 2018), but its high computational cost limits its practical applicability. In addition, emerging methods, such as those based on the Marchenko theory (Gu et al., 2023), and methods that suppress internal multiples in the image space (Berkhout and Verschuur, 2012; You and Cao, 2020; 2025), show promise, although the theoretical foundation remains underdeveloped.

The IME approach is developed based on the Surface-Related Multiple Elimination (SRME) method (Berkhout and Verschuur, 1997), which extends the data-driven convolutional strategy used for the prediction of surface-related multiples to that of internal multiples (Ypma and Verschuur, 2013). Berkhout (1997, 1999, 2005) proposed a method for predicting internal multiples using common-focus-point (CFP) gathers, and further developed both boundary and layer-related methods. However, the construction of CFP gathers requires prior velocity information, which constrains its practical applicability. Building on this foundation, Jakubowicz (1998) developed a method for internal multiple prediction through interference theory, employing correlation and convolution operations among three datasets to achieve the multiple prediction (van Borselen, 2002; Hung and Wang, 2012).

* Corresponding author.
E-mail address: lizhina00@163.com (Z.-N. Li).
Peer review under the responsibility of China University of Petroleum (Beijing).

https://doi.org/10.1016/j.petsci.2026.04.033
1995-8226/

Subsequently, Ikelle (2006) introduced the concept of “virtual event” to predict the internal multiples and reinterpreted the construction process of internal multiples. Although both approaches (Jakubowicz, 1998; Ikelle, 2006) provide intuitive explanations for internal multiple prediction based on propagation paths of waves, they lack mathematical and physical derivations, and their theoretical frameworks remain insufficiently developed. It is worth noting that both ISS and IME approaches adopt a “prediction-adaptive subtraction” strategy for internal multiple suppression, with their effectiveness largely dependent on the performance of the adaptive subtraction. However, this strategy suffers from inherent limitations. Since internal multiples often significantly overlap with primaries in shot records, the adaptive subtraction process, which is commonly based on the minimum energy assumption, can cause primary energy leakage into the internal multiples, leading to a loss of primary energy. This reduces both the accuracy of multiple suppression and the amplitude fidelity of the primaries.

To address this issue, Zhang and Staring (2018) proposed the Marchenko Multiple Elimination (MME) method, which enables high-precision prediction for the amplitude and phase of internal multiples based on Marchenko theory, without relying on prior velocity information. Building on this work, Zhang et al. (2019) developed the transmission compensated MME (T-MME) method by introducing a compensation mechanism for transmission losses in the primary reflections. Santos et al. (2021) reformulated the MME as a least-squares problem (LSMME), which circumvents the convergence requirement imposed by the Neumann series expansion. However, these methods heavily depend on the quality of source wavelet deconvolution and remain insufficiently mature.

Another approach to improving accuracy involves inversion-based method. Ypma and Verschuur (2013) extended the Estimation of Primaries by Sparse Inversion (EPSI), which was proposed by Groenestijn and Verschuur (2009) for surface-related multiple suppression, to the field of internal multiple suppression. This method estimates primaries by alternately inverting three parameters, including the response from all boundaries below the internal multiple generating boundary, the impulse response from the generating boundary itself, and the source wavelet. In this way, it avoids the primary energy loss caused by adaptive subtraction. Although the inversion-based method shows obvious advantages in amplitude fidelity of the primaries, this method suffers from instability in wavelet estimation (Bao et al., 2022), and the mutual influence among these inversion parameters in the alternating inversion process leads to limited adaptability.

Considering the incomplete theoretical derivations of conventional IME methods and leveraging the advantages of inversion, we establish a rigorous mathematical and physical foundation based on the well-known feedback model (Berkhout and Verschuur, 2005). Within this novel theoretical framework, we derive an analytical expression for internal multiple elimination and further propose an inversion-based Closed-Loop IME (CL-IME) method. The proposed CL-IME method builds on the derived analytical expression and formulates an objective function with a single inversion parameter, enabling high-precision estimation of internal multiples. The estimated internal multiples are then directly subtracted from the seismic records to achieve effective suppression. The CL-IME method does not rely on any prior velocity information and avoids the issues of traditional approaches that depend on adaptive subtraction and wavelet estimation. It can suppress internal multiples in a stable and effective manner while preventing primary energy loss, thereby providing a robust technical foundation for improving seismic imaging quality in complex geological settings.

2. Methodology

2.1. Feedback model for primaries and internal multiples

According to the WRW model proposed by Berkhout (1982), the propagation of primaries can be described as follows. The seismic wave generated by a source at the surface z_0 propagates downward to a reflection boundary at depth z_n, where it is reflected upward. The reflected wave then travels back to the surface z_0, and is ultimately recorded by a detector. A schematic illustration of this process is shown in Fig. 1.

The mathematical expression of this process in the frequency domain is given by:

$$\begin{aligned}\Delta\mathbf{P}_n(z_0,z_0)&=\mathbf{D}(z_0)\mathbf{W}(z_0,z_n)\mathbf{R}(z_n,z_n)\mathbf{W}(z_n,z_0)\mathbf{S}(z_0)\\&=\mathbf{D}(z_0)\Delta\mathbf{X}_n(z_0,z_0)\mathbf{S}(z_0)\end{aligned}\tag{1}$$

here, matrix $\Delta\mathbf{P}_n(z_0,z_0)$ denotes the primaries generated at the boundary z_n, and matrix $\mathbf{S}(z_0)$ represents the source wavelet. Matrices $\mathbf{W}(z_n,z_0)$ and $\mathbf{W}(z_0,z_n)$ are the downgoing- and upgoing-propagation operators between the surface z_0 and the boundary z_n, respectively. Matrix $\mathbf{R}(z_n,z_n)$ denotes the upward-reflection operator at the boundary z_n, and matrix $\mathbf{D}(z_0)$ represents the detector response. Matrix $\Delta\mathbf{X}_n(z_0,z_0)=\mathbf{W}(z_0,z_n)\mathbf{R}(z_n,z_n)\mathbf{W}(z_n,z_0)$ corresponds to the primary impulse response at boundary z_n.

Based on the WRW model, Berkhout and Verschuur (2005) systematically analyzed the propagation mechanisms of internal multiples. A feedback model for primaries and internal multiples was summarized using the boundary formulation, based on an analysis of the raypaths of internal multiples related to boundary z_n, as illustrated in Fig. 2.

Following the above feedback model, the boundary formulation for internal multiple suppression using the CFP-based method is derived. The expressions of internal multiples related to the boundary z_n are given as follows (Berkhout and Verschuur, 2005):

$$\Delta\mathbf{M}_n(z_0,z_0)=\mathbf{D}(z_0)\{\overline{\mathbf{X}}(z_0,z_n)\}_n\mathbf{R}^{\wedge}(z_n,z_n)\{\overline{\mathbf{P}}^{-}(z_n,z_0)\}_{n-1}\quad\text{(model driven)}\tag{2a}$$

or as

$$\Delta\mathbf{M}_n(z_0,z_0)=\{\overline{\mathbf{P}}(z_0,z_n)\}_n\mathbf{A}(z_n,z_n)\{\overline{\mathbf{P}}(z_n,z_0)\}_{n-1}\text{(data driven)}\tag{2b}$$

Here, $\Delta\mathbf{M}_n(z_0,z_0)$ denotes the internal multiples related to the target boundary at depth z_n. $\mathbf{A}(z_n,z_n)$ and $\mathbf{R}^{\wedge}(z_n,z_n)$ are the boundary operator and the downward-reflection operator at boundary z_n, respectively. $\mathbf{P}$ represents the seismic record. $\{\ \}_{n-1}$

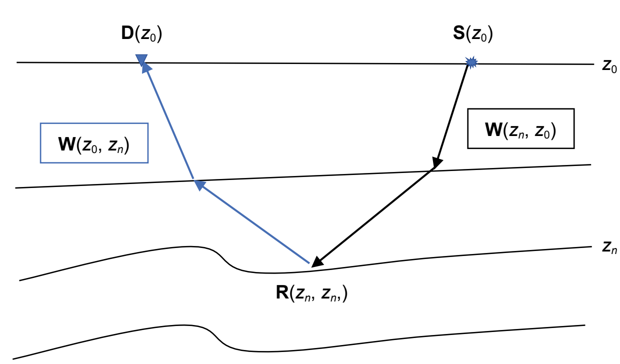

Fig. 1. WRW model.

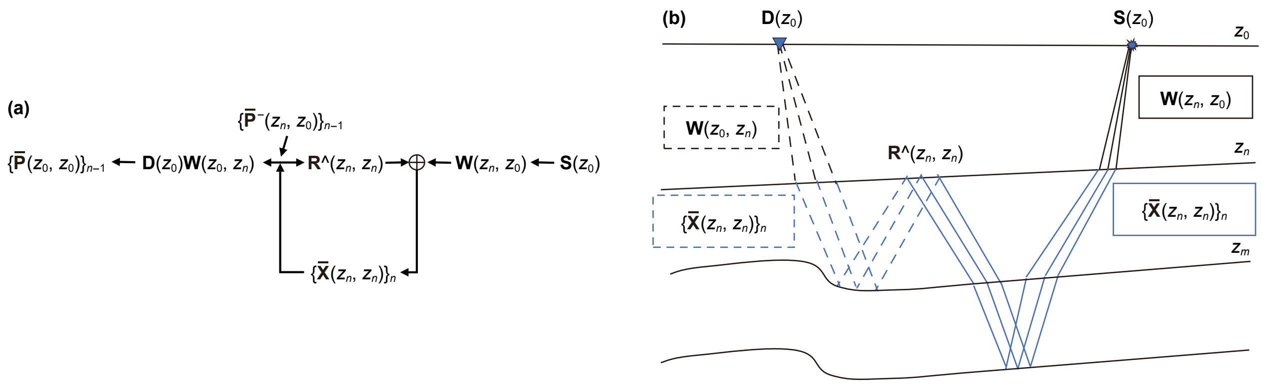

Fig. 2. Feedback model and raypath illustration. **(a)** Feedback model for primaries and internal multiples using the boundary formulation, **(b)** raypaths for internal multiples related to boundary z_n.

signifies that internal multiples related to boundaries at or above depth z_{n-1} (i.e., $z \le z_{n-1}$) have been removed, while those related to deeper boundaries (i.e., $z > z_{n-1}$) remain in the data. The overbar on $\overline{\mathbf{P}}$ indicates that all primary reflections related to the target boundary z_n and shallower boundaries (i.e., $z \le z_n$) have been muted. $\{\overline{\mathbf{X}}(z_n, z_n)\}_n$ denotes the impulse response in a half-space $z > z_n$. Additionally, the minus sign in $\overline{\mathbf{P}}^-$ represents the upgoing wavefield. Based on these definitions, the wavefield $\{\overline{\mathbf{P}}(z_n, z_0)\}_{n-1}$ can be expressed as follows:

$$\{\overline{\mathbf{P}}(z_n, z_0)\}_{n-1} = \mathbf{D}(z_n)\{\overline{\mathbf{P}}^-(z_n, z_0)\}_{n-1} \tag{3}$$

According to the WRW model, the following equation can be concluded:

$$\{\overline{\mathbf{P}}(z_0, z_n)\}_n = \mathbf{D}(z_0)\{\overline{\mathbf{X}}(z_0, z_n)\}_n \mathbf{S}(z_n) \tag{4}$$

By substituting Eqs. (3) and (4) into Eq. (2b) and comparing the result with Eq. (2a), the boundary operator can be explicitly expressed as:

$$\mathbf{A}(z_n, z_n) = \mathbf{S}^{-1}(z_n)\mathbf{R}^{\wedge}(z_n, z_n)\mathbf{D}^{-1}(z_n) \tag{5}$$

2.2. Internal multiple elimination based on the feedback model

In the existing data-driven formulation of internal multiples related to boundary z_n (Eq. (2b)), the prediction of internal multiples relies on the data matrices $\{\overline{\mathbf{P}}(z_0, z_n)\}_n$ and $\{\overline{\mathbf{P}}(z_n, z_0)\}_{n-1}$, which are obtained through the construction of the CFP gathers, a process that requires prior velocity information.

Building upon the aforementioned equations and the WRW model, we derive a novel theoretical framework for predicting and suppressing internal multiples driven by surface seismic data. Unlike conventional CFP-based method, the proposed method does not require the construction of CFP gathers, thereby eliminating the dependence on prior velocity information and enhancing its applicability in practical data processing. Moreover, this method is derived from the theory of wavefield propagation and provides a new perspective for internal multiple suppression based on the feedback model. It overcomes the limitations of traditional IME methods (e.g., Jakubowicz, 1998; Ikelle, 2006) that rely exclusively on raypath analysis and lack rigorous mathematical and physical foundations. As a result, this method improves and extends the current theoretical framework for internal multiple suppression.

Based on the WRW model, we represent the wavefield $\mathbf{P}(z_0, z_n)$ in Eq. (2b) using seismic records $\mathbf{P}(z_0, z_0)$ acquired with both sources and detectors located at the surface, leading to the following expression:

$$\{\overline{\mathbf{P}}(z_0, z_n)\}_n = \{\overline{\mathbf{P}}(z_0, z_0)\}_n \mathbf{S}^{-1}(z_0)\mathbf{W}^{-1}(z_n, z_0)\mathbf{S}(z_n) \tag{6}$$

It can be seen that the above equation eliminates the source effect at the surface z_0 using $\mathbf{S}^{-1}(z_0)$, removes the propagation effect from surface z_0 to boundary z_n by applying $\mathbf{W}^{-1}(z_n, z_0)$, and places the sources at the boundary z_n through the application of $\mathbf{S}(z_n)$, which is virtual, thereby achieving the transformation from $\mathbf{P}(z_0, z_0)$ to $\mathbf{P}(z_0, z_n)$.

Similarly,

$$\{\overline{\mathbf{P}}(z_n, z_0)\}_{n-1} = \mathbf{D}(z_n)\mathbf{W}^{-1}(z_0, z_n)\mathbf{D}^{-1}(z_0)\{\overline{\mathbf{P}}(z_0, z_0)\}_{n-1} \tag{7}$$

To obtain a prediction expression for internal multiples $\Delta\mathbf{M}_n(z_0, z_0)$ that relies solely on seismic data acquired with both sources and detectors located at the surface, Eqs. (6) and (7) are substituted into Eq. (2b), yielding:

$$\Delta\mathbf{M}_n(z_0, z_0) = \{\overline{\mathbf{P}}(z_0, z_0)\}_n \mathbf{S}^{-1}(z_0)\mathbf{W}^{-1}(z_n, z_0)\mathbf{S}(z_n)\mathbf{A}(z_n, z_n) \mathbf{D}(z_n)\mathbf{W}^{-1}(z_0, z_n)\mathbf{D}^{-1}(z_0)\{\overline{\mathbf{P}}(z_0, z_0)\}_{n-1} \tag{8}$$

By substituting the boundary operator expression $\mathbf{A}(z_n, z_n)$ (Eq. (5)) into Eq. (8), we further obtain:

$$\begin{aligned}\Delta\mathbf{M}_n(z_0, z_0) &= \{\overline{\mathbf{P}}(z_0, z_0)\}_n \mathbf{S}^{-1}(z_0)\mathbf{W}^{-1}(z_n, z_0)\mathbf{R}^{\wedge}(z_n, z_n) \mathbf{W}^{-1}(z_0, z_n)\mathbf{D}^{-1}(z_0)\{\overline{\mathbf{P}}(z_0, z_0)\}_{n-1} = \{\overline{\mathbf{P}}(z_0, z_0)\}_n \mathbf{S}^{-1}(z_0) \\ &\quad \mathbf{W}^{-1}(z_n, z_0)\mathbf{R}^{\wedge}(z_n, z_n)\mathbf{R}(z_n, z_n)\mathbf{R}^{-1}(z_n, z_n)\mathbf{W}^{-1}(z_0, z_n) \mathbf{D}^{-1}(z_0)\{\overline{\mathbf{P}}(z_0, z_0)\}_{n-1}\end{aligned} \tag{9}$$

To ensure numerical stability, we adopt the conjugate transpose of the matrix as a stable approximation of its inverse, preserving the travel-time information (Berkhout, 1997). Accordingly, Eq. (9) can be rewritten as:

$$\Delta\mathbf{M}_n(z_0, z_0) \approx \{\overline{\mathbf{P}}(z_0, z_0)\}_n \mathbf{S}^{\mathrm{H}}(z_0)\mathbf{W}^{\mathrm{H}}(z_n, z_0)\mathbf{R}^{\wedge}(z_n, z_n)\mathbf{R}(z_n, z_n) \mathbf{R}^{\mathrm{H}}(z_n, z_n)\mathbf{W}^{\mathrm{H}}(z_0, z_n)\mathbf{D}^{\mathrm{H}}(z_0)\{\overline{\mathbf{P}}(z_0, z_0)\}_{n-1} \tag{10}$$

To simplify the expression of internal multiples $\Delta\mathbf{M}_n(z_0, z_0)$, it is assumed that the detector response $\mathbf{D}$ and source wavelet $\mathbf{S}$ are angle-independent, i.e., their directional characteristics are neglected (Thorbecke, 1997). Under this assumption, both $\mathbf{D}$ and $\mathbf{S}$ can be represented as diagonal matrices, such that $\mathbf{D} = D(\omega)\mathbf{I}$, $\mathbf{S} = S(\omega)\mathbf{I}$.

Meanwhile, it is assumed that $\mathbf{W}(z_n,z_0)$, $\mathbf{R}^{\wedge}(z_n,z_n)$, and $\mathbf{R}(z_n,z_n)$ are Toeplitz matrices, which implies that the reflection and propagation properties are laterally invariant (Thorbecke, 1997). Similarly, $\mathbf{W}^{\mathrm{H}}(z_n,z_0)$ is also considered as a Toeplitz matrix. As a result, $\mathbf{W}^{\mathrm{H}}(z_n, z_0)$, $\mathbf{R}^{\wedge}(z_n, z_n)$, and $\mathbf{R}(z_n,z_n)$ can be interchanged (Thorbecke, 1997). Under these assumptions, Eq. (10) can be further expressed as:

$$\Delta\mathbf{M}_n(z_0,z_0) \approx \{\overline{\mathbf{P}}(z_0,z_0)\}_n[\mathbf{R}^{\wedge}(z_n,z_n)\mathbf{R}(z_n,z_n)][\mathbf{D}(z_0)\mathbf{W}(z_0,z_n)\mathbf{R}(z_n,z_n)\mathbf{W}(z_n,z_0)\mathbf{S}(z_0)]^{\mathrm{H}}\{\overline{\mathbf{P}}(z_0,z_0)\}_{n-1} \tag{11}$$

According to Eq. (1), Eq. (11) can be further reformulated as:

$$\Delta\mathbf{M}_n(z_0,z_0)\approx\{\overline{\mathbf{P}}(z_0,z_0)\}_n[\mathbf{R}^{\wedge}(z_n,z_n)\mathbf{R}(z_n,z_n)]\Delta\mathbf{P}_n{}^{\mathrm{H}}(z_0,z_0)\{\overline{\mathbf{P}}(z_0,z_0)\}_{n-1} \tag{12}$$

By defining a new boundary operator $\mathbf{A}'(z_n,\ z_n) = \mathbf{R}^{\wedge}(z_n, z_n)\mathbf{R}(z_n, z_n)$, Eq. (12) can be expressed as:

$$\Delta\mathbf{M}_n(z_0,z_0)=\{\overline{\mathbf{P}}(z_0,z_0)\}_n\mathbf{A}'(z_n,z_n)\Delta\mathbf{P}_n{}^{\mathrm{H}}(z_0,z_0)\{\overline{\mathbf{P}}(z_0,z_0)\}_{n-1} \tag{13}$$

As indicated, the prediction of internal multiples $\Delta\mathbf{M}_n(z_0,z_0)$ relies on three data matrices: $\{\overline{\mathbf{P}}(z_0,z_0)\}_n$, $\Delta\mathbf{P}_n(z_0,\ z_0)$, and $\{\overline{\mathbf{P}}(z_0,z_0)\}_{n-1}$, whose source and detector locations are all located on the surface. Consequently, the construction of the CFP gathers is no longer required. Moreover, the boundary operator $\mathbf{A}'(z_n,z_n)$ is associated with the reflection characteristics of the boundary z_n, representing a novel and significant finding that distinguishes it from existing IME methods, which lack rigorous theoretical derivation.

It is worth noting that $\{\overline{\mathbf{P}}(z_0,z_0)\}_n$ represents the seismic record in which both internal multiples and all primaries related to boundaries at depths $z \le z_n$ have been removed. In contrast, $\{\overline{\mathbf{P}}(z_0,z_0)\}_{n-1}$ denotes the seismic record in which both internal multiples related to boundaries at depths $z \le z_{n-1}$, as well as primaries related to boundaries at depths $z \le z_n$ have been removed. Therefore, the following relationship holds:

$$\{\overline{\mathbf{P}}(z_0,z_0)\}_n=\{\overline{\mathbf{P}}(z_0,z_0)\}_{n-1}-\Delta\mathbf{M}_n(z_0,z_0) \tag{14}$$

In summary, the internal multiple suppression method based on the feedback model can be expressed by the following equations:

$$\begin{cases}\{\overline{\mathbf{P}}\}_n{}^i = \{\overline{\mathbf{P}}\}_{n-1} - \Delta\mathbf{M}_n{}^i \\ \Delta\mathbf{M}_n{}^i = \{\overline{\mathbf{P}}\}_n{}^{i-1}\mathbf{A}'\Delta\mathbf{P}_n{}^{\mathrm{H}}\{\overline{\mathbf{P}}\}_{n-1} \\ \{\overline{\mathbf{P}}\}_n{}^0 = \{\overline{\mathbf{P}}\}_{n-1}\end{cases} \tag{15}$$

For conciseness, location variables have been omitted. The defined boundary operator $\mathbf{A}'$ can be computed by solving the following least-squares problem with a Frobenius L_2-norm:

$$\left\|\{\overline{\mathbf{P}}\}_{n-1}-\Delta\mathbf{M}_n\right\|^2=\left\|\{\overline{\mathbf{P}}\}_{n-1}-\{\overline{\mathbf{P}}\}_n\mathbf{A}'\Delta\mathbf{P}_n{}^{\mathrm{H}}\{\overline{\mathbf{P}}\}_{n-1}\right\|^2\rightarrow\min \tag{16}$$

According to the above derivation, the workflow for internal multiple suppression using the feedback model can be summarized as follows: (1) Mute $\{\mathbf{P}\}_{n-1}$ to obtain $\Delta\mathbf{P}_n$ and $\{\overline{\mathbf{P}}\}_{n-1}$; (2) Calculate the predicted internal multiples $\Delta\mathbf{M}_{n\_\mathrm{pre}}$ using equation $\Delta\mathbf{M}_{n\_\mathrm{pre}}=\{\overline{\mathbf{P}}\}_n\Delta\mathbf{P}_n{}^{\mathrm{H}}\{\overline{\mathbf{P}}\}_{n-1}$, with the initial iteration set as $\{\overline{\mathbf{P}}\}_n = \{\overline{\mathbf{P}}\}_{n-1}$; (3) Apply adaptive subtraction between $\{\overline{\mathbf{P}}\}_{n-1}$ and $\Delta\mathbf{M}_{n\_\mathrm{pre}}$ based on Eq. (16) to obtain $\{\overline{\mathbf{P}}\}_n$; (4) Repeat steps (2)–(3) with the updated $\{\overline{\mathbf{P}}\}_n$ until a satisfactory estimation of the internal multiples $\Delta\mathbf{M}_n$ is achieved; (5) Obtain the final result $\{\mathbf{P}\}_n$ after multiple suppression using Eq. (17):

$$\{\mathbf{P}\}_n=\{\mathbf{P}\}_{n-1}-\Delta\mathbf{M}_n \tag{17}$$

Once the wavefield $\{\mathbf{P}\}_n$ is obtained, the data $\{\overline{\mathbf{P}}\}_n$ and $\Delta\mathbf{P}_{n+1}$ related to the next selected reflecting boundary z_{n+1} can be extracted. It should be noted that, the overbar on $\{\overline{\mathbf{P}}\}_n$ indicates that all primary reflections at or above the target boundary z_{n+1} (i.e., $z \le z_{n+1}$) have been muted. By repeating the above procedure, internal multiples related to boundary z_{n+1} can be further suppressed, thereby achieving a layer-by-layer internal multiple suppression.

The above internal multiple suppression method derived from the feedback model is implemented in a manner similar to existing IME approaches (Jakubowicz, 1998; Ikelle, 2006), in which internal multiples are predicted through convolution operations between datasets and subsequently suppressed by adaptive subtraction, without requiring any priori velocity information. However, these existing methods derive the internal multiple prediction formulas exclusively from propagation-path analysis, yet lack a comprehensive theoretical derivation, while the present study establishes a comprehensive theoretical framework grounded in the feedback model and derives an explicit expression for the boundary operator $\mathbf{A}'$, thereby providing a significant theoretical advancement.

Similar to the existing IME approaches, when internal multiples overlap with primaries, the adaptive subtraction in the derived method may also cause primary energy loss, thereby limiting the accuracy of internal multiple suppression. Therefore, it is imperative to develop a new internal multiple suppression method with higher suppression accuracy to deal with this issue.

2.3. Closed-loop internal multiple elimination

To address primary energy loss caused by adaptive subtraction, this study incorporates the inversion concept into the derived internal multiple suppression formulas and proposes a Closed-Loop Internal Multiple Elimination (CL-IME) method. In this method, an objective function is formulated for the wavefield $\{\overline{\mathbf{P}}\}_n$, which is directly inverted by minimizing the objective function, thereby avoiding the adaptive subtraction. As a result, more accurate internal multiples can be estimated, achieving higher-precision internal multiple suppression while effectively preserving primary energy.

From Eq. (15), it follows that:

$$\begin{aligned}\{\overline{\mathbf{P}}\}_{n-1} &= \{\overline{\mathbf{P}}\}_n + \{\overline{\mathbf{P}}\}_n\mathbf{A}'\Delta\mathbf{P}_n{}^{\mathrm{H}}\{\overline{\mathbf{P}}\}_{n-1} \\ &= \{\overline{\mathbf{P}}\}_n\left(\mathbf{I}+\mathbf{A}'\Delta\mathbf{P}_n{}^{\mathrm{H}}\{\overline{\mathbf{P}}\}_{n-1}\right)\end{aligned} \tag{18}$$

In order to estimate $\{\overline{\mathbf{P}}\}_n$ from $\{\overline{\mathbf{P}}\}_{n-1}$, an objective function J is constructed to quantify the difference between the computed wavefield (sum of the wavefield $\{\overline{\mathbf{P}}\}_n$ and the internal multiples $\Delta\mathbf{M}_n$) and the wavefield $\{\overline{\mathbf{P}}\}_{n-1}$ obtained from the observed data. The objective function is formulated as a Frobenius L_2 norm, defined as:

$$J=\sum_{\omega}J_{\omega}=\sum_{\omega}\left\|\{\overline{\mathbf{P}}\}_{n-1}-\widehat{\{\overline{\mathbf{P}}\}}_n\left(\mathbf{I}+\widehat{\mathbf{A}'}\Delta\mathbf{P}_n{}^{\mathrm{H}}\{\overline{\mathbf{P}}\}_{n-1}\right)\right\|^2 \tag{19}$$

where $\widehat{\{\overline{\mathbf{P}}\}}_n$ and $\widehat{\mathbf{A}'}$ represent the estimations of $\{\overline{\mathbf{P}}\}_n$ and $\mathbf{A}'$, respectively. The initial values are set as $\widehat{\{\overline{\mathbf{P}}\}}_n=0$ and $\widehat{\mathbf{A}'}=0$. By minimizing the objective function J_ω, $\widehat{\{\overline{\mathbf{P}}\}}_n$ and $\widehat{\mathbf{A}'}$ are iteratively updated, such that the sum of the estimated wavefield $\{\overline{\mathbf{P}}\}_n$ and the estimated internal multiples $\Delta\mathbf{M}_n$ increasingly approximates the wavefield $\{\overline{\mathbf{P}}\}_{n-1}$. In this way, both the estimated wavefield $\{\overline{\mathbf{P}}\}_n$ and the estimated internal multiples $\Delta\mathbf{M}_n$ become progressively more accurate.

To solve the above least-square problem, a first-order Taylor expansion of J_ω is used to determine the appropriate descent direction for updating the inverted wavefield $\{\overline{\mathbf{P}}\}_n$. This descent direction is obtained from the extremum condition of J, $\nabla_{\widehat{\{\overline{\mathbf{P}}\}}_n}J_\omega(\{\overline{\mathbf{P}}\}_n,\mathbf{A}')=0$, yielding the gradient of inverted wavefield $\Delta\{\overline{\mathbf{P}}\}_n=-\nabla_{\widehat{\{\overline{\mathbf{P}}\}}_n}J_\omega(\{\overline{\mathbf{P}}\}_n,\mathbf{A}')$, which can be expressed as:

$$\begin{aligned}\Delta\{\overline{\mathbf{P}}\}_n=&\Big[\{\overline{\mathbf{P}}\}_{n-1}-\widehat{\{\overline{\mathbf{P}}\}}_n\Big(\mathbf{I}\\&+\widehat{\mathbf{A}'}\Delta\mathbf{P}_n{}^{\mathrm{H}}\{\overline{\mathbf{P}}\}_{n-1}\Big)\Big]\Big(\mathbf{I}+\widehat{\mathbf{A}'}\Delta\mathbf{P}_n{}^{\mathrm{H}}\{\overline{\mathbf{P}}\}_{n-1}\Big)^{\mathrm{H}}\end{aligned} \tag{20}$$

The boundary operator $\mathbf{A}'$ is estimated according to Eq. (16). Based on the gradient $\Delta\{\overline{\mathbf{P}}\}_n$ and step length α, the update formula for the wavefield $\{\overline{\mathbf{P}}\}_n$ can be given by:

$$\widehat{\{\overline{\mathbf{P}}\}}_n^{(i+1)}=\widehat{\{\overline{\mathbf{P}}\}}_n^{(i)}+\alpha\boldsymbol{\Delta}\{\overline{\mathbf{P}}\}_n^{(i)} \tag{21}$$

The step length α is determined via a line search, which ensures that $J(\widehat{\{\overline{\mathbf{P}}\}}_n+\alpha\boldsymbol{\Delta}\{\overline{\mathbf{P}}\}_n)\rightarrow\min$. Specifically:

$$\begin{aligned}J(\widehat{\{\overline{\mathbf{P}}\}}_n+\alpha\boldsymbol{\Delta}\{\overline{\mathbf{P}}\}_n)&=\sum_{\omega}\left\|\{\overline{\mathbf{P}}\}_{n-1}-\widehat{\{\overline{\mathbf{P}}\}}_n\left(\mathbf{I}+\widehat{\mathbf{A}'}\Delta\mathbf{P}_n{}^{\mathrm{H}}\{\overline{\mathbf{P}}\}_{n-1}\right)-\alpha\boldsymbol{\Delta}\{\overline{\mathbf{P}}\}_n\left(\mathbf{I}+\widehat{\mathbf{A}'}\Delta\mathbf{P}_n{}^{\mathrm{H}}\{\overline{\mathbf{P}}\}_{n-1}\right)\right\|^2=\sum_{\omega}\|\mathbf{V}-\alpha\mathbf{K}\|^2\\&=\sum_{\omega}\mathrm{Tr}(\mathbf{V}-\alpha\mathbf{K})^{\mathrm{H}}(\mathbf{V}-\alpha\mathbf{K})=\sum_{\omega}\mathrm{Tr}\left(\mathbf{V}^{\mathrm{H}}\mathbf{V}+\alpha^2\mathbf{K}^{\mathrm{H}}\mathbf{K}-\alpha\mathbf{V}^{\mathrm{H}}\mathbf{K}-\alpha\mathbf{K}^{\mathrm{H}}\mathbf{V}\right)\end{aligned} \tag{22}$$

With

$$\begin{cases}\mathbf{V}=\{\overline{\mathbf{P}}\}_{n-1}-\widehat{\{\overline{\mathbf{P}}\}}_n\left(\mathbf{I}+\widehat{\mathbf{A}'}\Delta\mathbf{P}_n{}^{\mathrm{H}}\{\overline{\mathbf{P}}\}_{n-1}\right)\\ \mathbf{K}=\boldsymbol{\Delta}\{\overline{\mathbf{P}}\}_n\left(\mathbf{I}+\widehat{\mathbf{A}'}\Delta\mathbf{P}_n{}^{\mathrm{H}}\{\overline{\mathbf{P}}\}_{n-1}\right)\end{cases} \tag{23}$$

To achieve $J(\widehat{\{\overline{\mathbf{P}}\}}_n+\alpha\Delta\{\overline{\mathbf{P}}\}_n)\rightarrow\min$, the extremum condition $\frac{\mathrm{d}J(\widehat{\{\overline{\mathbf{P}}\}}_n+\alpha\Delta\{\overline{\mathbf{P}}\}_n)}{\mathrm{d}\alpha}=0$ is applied, yielding:

$$\alpha=\frac{\sum_{\omega}\left(\mathrm{Tr}\left(\mathbf{V}^{\mathrm{H}}\mathbf{K}\right)+\mathrm{Tr}\left(\mathbf{K}^{\mathrm{H}}\mathbf{V}\right)\right)}{2\sum_{\omega}\mathrm{Tr}\left(\mathbf{K}^{\mathrm{H}}\mathbf{K}\right)} \tag{24}$$

Since the step length α is a real number, any imaginary part introduced by numerical computation is neglected. Furthermore, noting that $\mathrm{Re}\left(\mathrm{Tr}\left(\mathbf{V}^{\mathrm{H}}\mathbf{K}\right)\right)=\mathrm{Re}\left(\mathrm{Tr}\left(\mathbf{K}^{\mathrm{H}}\mathbf{V}\right)\right)$, α can be rewritten in a real-valued form:

$$\alpha=\frac{\sum_{\omega}\mathrm{Re}\left(\mathrm{Tr}\left(\mathbf{V}^{\mathrm{H}}\mathbf{K}\right)\right)}{\sum_{\omega}\mathrm{Tr}\left(\mathbf{K}^{\mathrm{H}}\mathbf{K}\right)} \tag{25}$$

Through the above inversion process, the wavefield $\{\overline{\mathbf{P}}\}_n$ can be directly estimated without relying on the adaptive subtraction, thereby ensuring the accuracy of internal multiple separation:

$$\Delta\mathbf{M}_n=\{\overline{\mathbf{P}}\}_{n-1}-\{\overline{\mathbf{P}}\}_n \tag{26}$$

Subsequently, the result $\{\mathbf{P}\}_n$ after suppressing the internal multiples related to boundary z_n can be obtained using Eq. (17). Similarly, the wavefields $\Delta\mathbf{P}_{n+1}$ and $\{\overline{\mathbf{P}}\}_n$ corresponding to the next reflection boundary z_{n+1} can be obtained, and the above procedure is repeated to further suppress internal multiples related to boundary z_{n+1}. By proceeding layer by layer in this manner, the internal multiple suppression can be achieved throughout the subsurface.

Overall, the CL-IME can be regarded as an “inversion-oriented” or “closed-loop” version of the internal multiple suppression method based on the feedback model. It iteratively updates the inverted wavefields by computing gradients and step lengths, enabling accurate estimation of internal multiples and ultimately achieving high-precision suppression of these multiples.

3. Numerical examples

In this section, numerical tests of the proposed CL-IME are performed and compared with the internal multiple suppression method based on the feedback model to validate its effectiveness, adaptability, and superiority.

It should be noted that the derived internal multiple suppression method based on the feedback model, similar to existing IME approaches, predicts internal multiples through convolution operations between the datasets and can therefore be regarded as a new IME approach. For conciseness, the term “IME” hereafter specifically refers to this derived method.

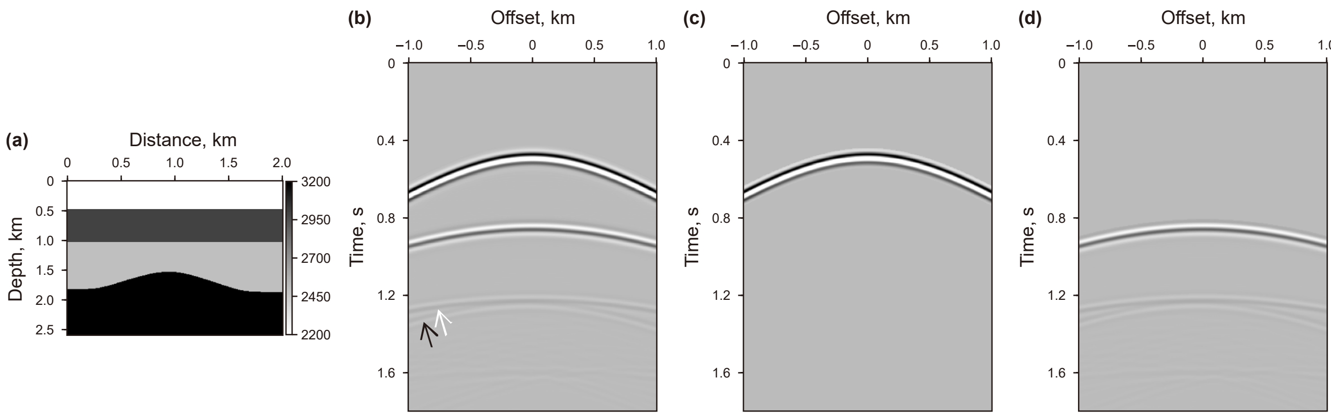

Fig. 3. Simple model and data preparation. **(a)** Velocity model, **(b)** seismic record $\{\mathbf{P}\}_0$, **(c)** primaries $\Delta\mathbf{P}_1$, **(d)** wavefield $\{\overline{\mathbf{P}}\}_0$.

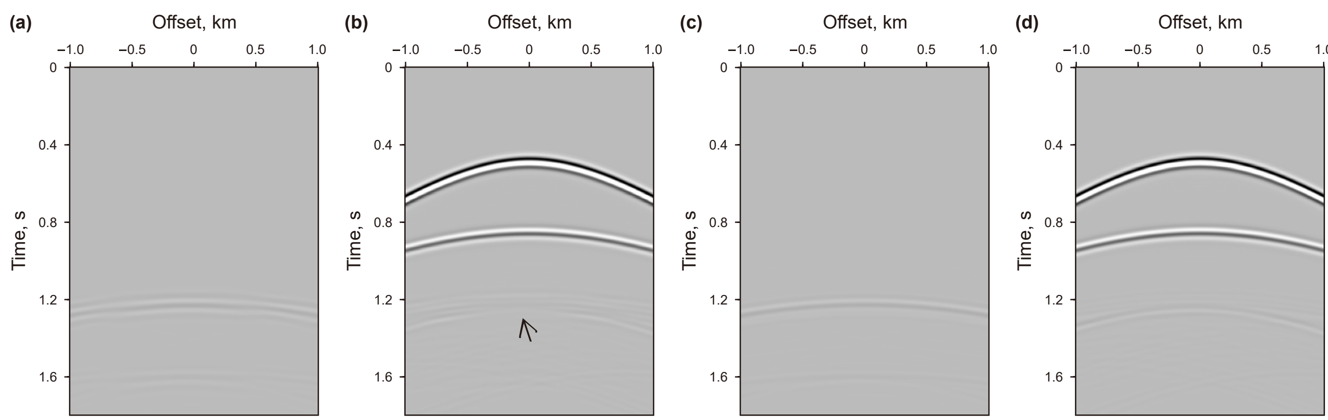

Fig. 4. Suppression results of internal multiples. **(a)** Internal multiples calculated by IME, **(b)** suppression result of IME, **(c)** internal multiples estimated by CL-IME, **(d)** suppression result of CL-IME.

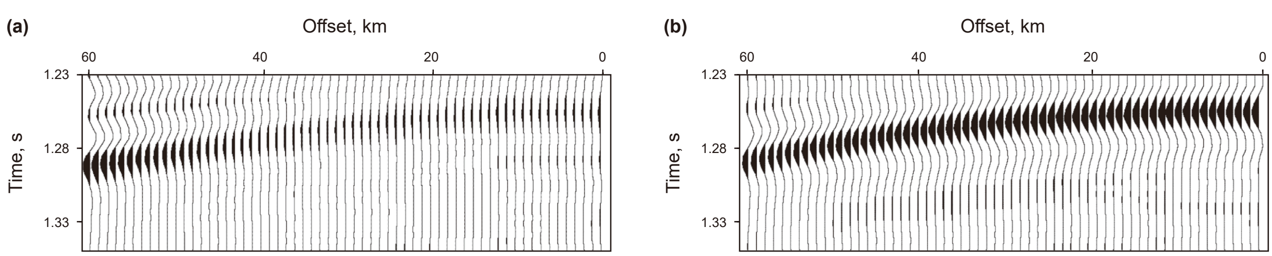

Fig. 5. Local waveform comparison in internal multiple suppression results. **(a)** IME, **(b)** CL-IME.

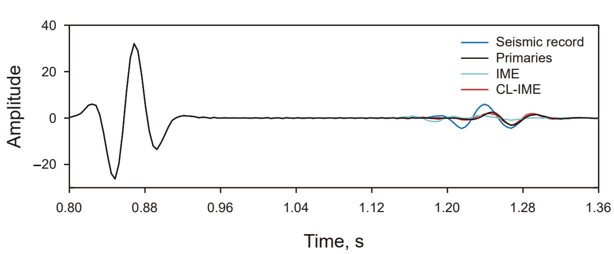

Fig. 6. Comparison of single-trace waveforms.

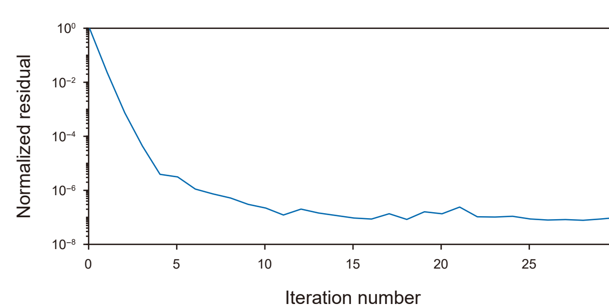

Fig. 7. Convergence curve of CL-IME.

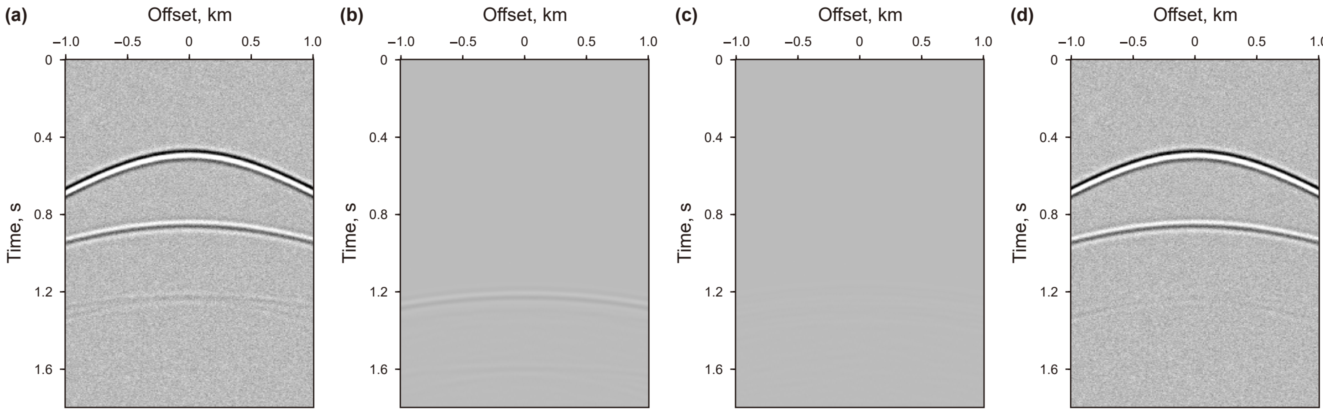

Fig. 8. Internal multiple suppression results of CL-IME under noisy conditions. **(a)** Seismic record with noise, **(b)** internal multiples estimated by CL-IME, **(c)** difference between the estimated internal multiples under noisy and noise-free conditions, **(d)** suppression result of CL-IME.

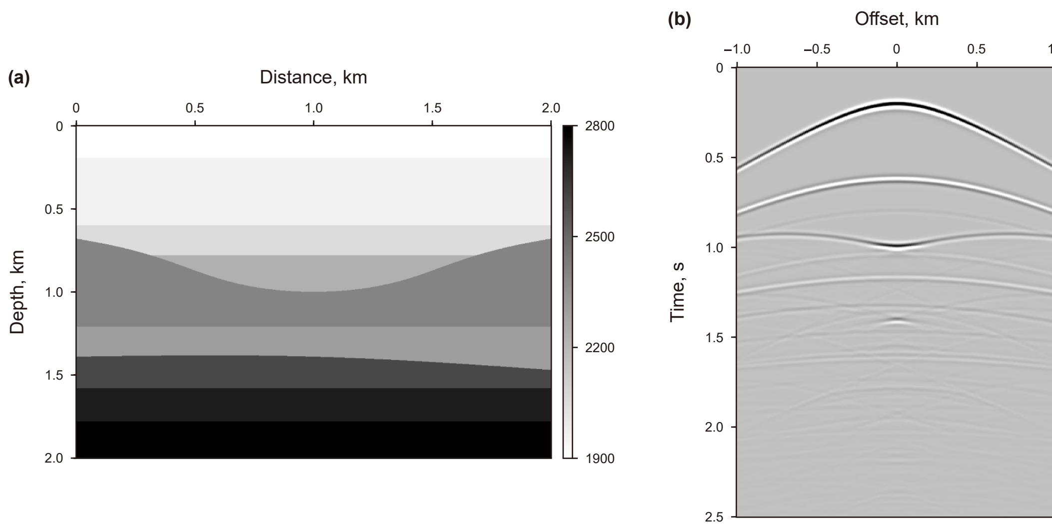

Fig. 9. Complex model. **(a)** Velocity model, **(b)** seismic record.

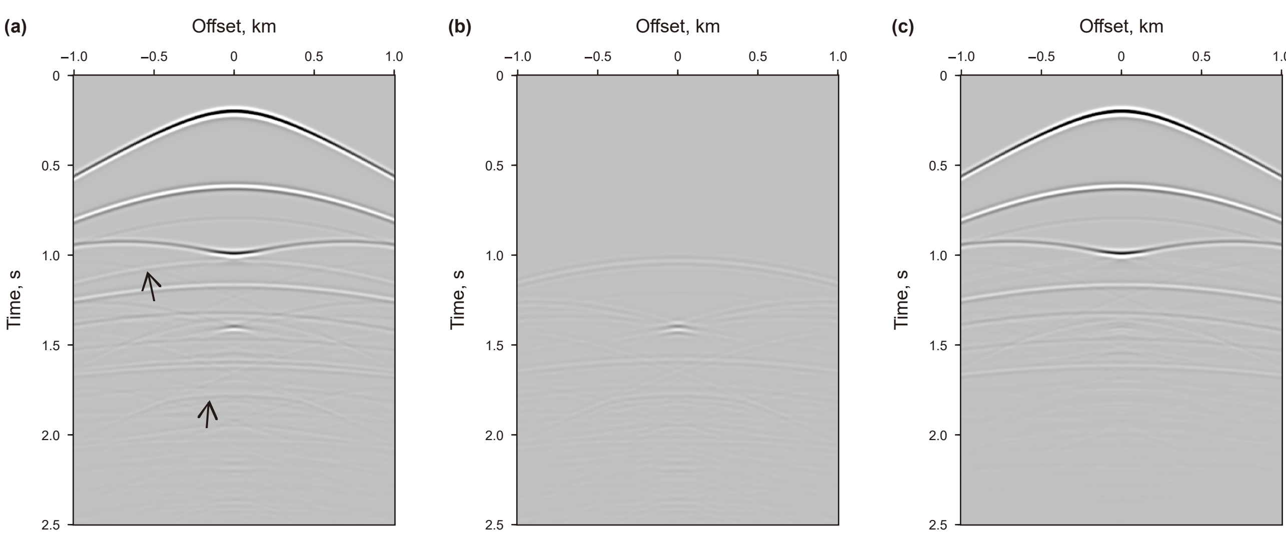

Fig. 10. Suppression of internal multiples related to the first boundary using CL-IME. **(a)** Seismic record, **(b)** estimation of internal multiples $\Delta\mathbf{M}_1$, **(c)** multiples $\Delta\mathbf{M}_1$ suppression result.

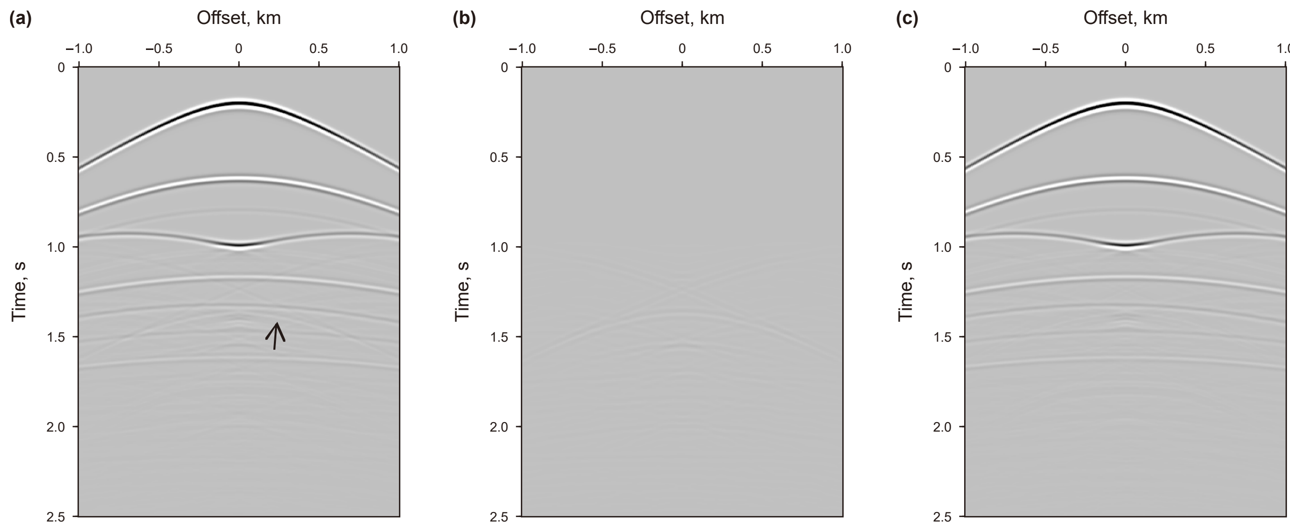

Fig. 11. Suppression of internal multiples related to the second boundary using CL-IME. **(a)** Multiples $\Delta\mathbf{M}_1$ suppression result, **(b)** estimation of internal multiples $\Delta\mathbf{M}_2$, **(c)** multiples $\Delta\mathbf{M}_2$ suppression result.

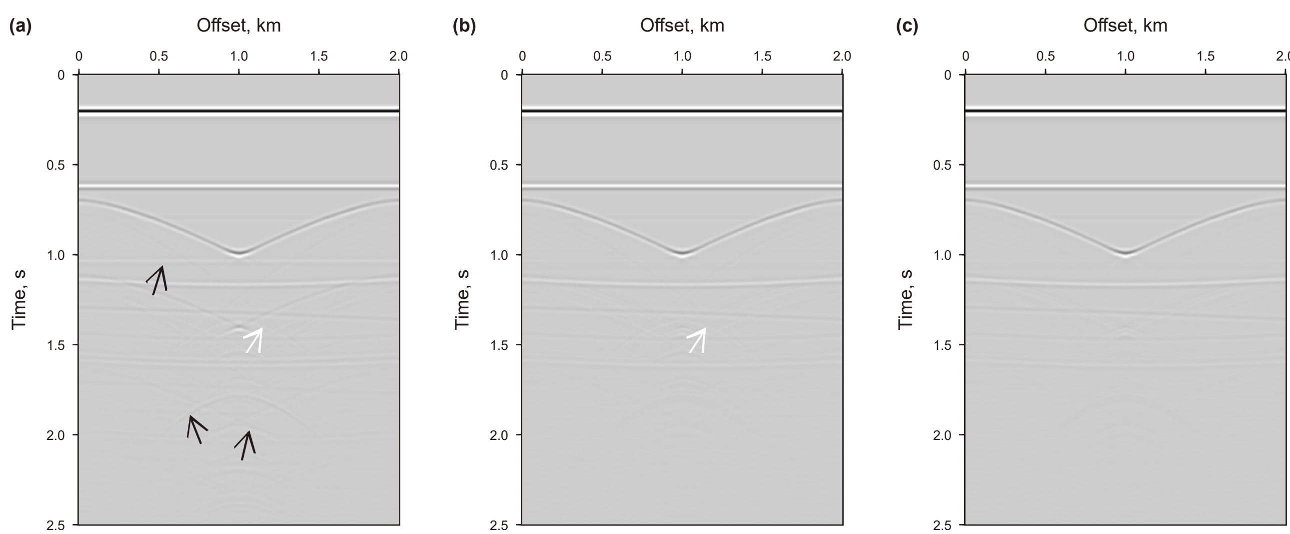

Fig. 12. Comparison of zero-offset sections. **(a)** Zero-offset section of seismic record, **(b)** zero-offset section after suppression of internal multiples related to first boundary, **(c)** zero-offset after suppression of internal multiples related to the second boundary.

3.1. Simple model

First, the IME and CL-IME methods are tested using seismic records generated from a simple velocity model (Fig. 3(a)). There are 201 sources and 201 detectors evenly spaced along the surface with a spacing of 10 m interval. The recording time is 1.8 s with a sampling interval of 4 ms. An absorbing boundary condition is applied to simulate data without surface-related multiples, and the shot records can be represented as $\{\mathbf{P}\}_0$.

A single shot is selected for demonstration (Fig. 3(b)). The analysis on the velocity model indicates that the shot record contains only internal multiples related to the first boundary z_1 (white arrow), which significantly overlap with the primaries generated from the third boundary z_3 (black arrow). In this case, with the target boundary set at z_1, the primaries $\Delta\mathbf{P}_1$ generated from z_1 (Fig. 3(c)) and the wavefield $\{\overline{\mathbf{P}}\}_0$ (Fig. 3(d)) are separated from the seismic record $\{\mathbf{P}\}_0$.

Based on the separated data, the IME and CL-IME methods are then applied to suppress the internal multiples $\Delta\mathbf{M}_1$. The results are shown in Fig. 4. As seen in Fig. 4(a), the internal multiples calculated by the IME method generally match the location and shape of the internal multiples in the shot records. The suppression result of IME (Fig. 4(b)) indicates that the internal multiples are attenuated, confirming the effectiveness of the IME method. However, the internal multiples (Fig. 4(a)) exhibit uneven energy distribution, and in regions where primaries and multiples overlap, significant primary energy leakage occurs. This issue is further highlighted in the suppression results (Fig. 4(b)): in the overlapping regions, the adaptive subtraction causes obvious primary energy loss (black arrow). In contrast, the internal multiples estimated by CL-IME (Fig. 4(c)) exhibit a uniform energy distribution, and their waveforms closely match those in the seismic record, demonstrating that CL-IME provides more accurate estimates of internal multiples. Effective suppression of the internal multiples

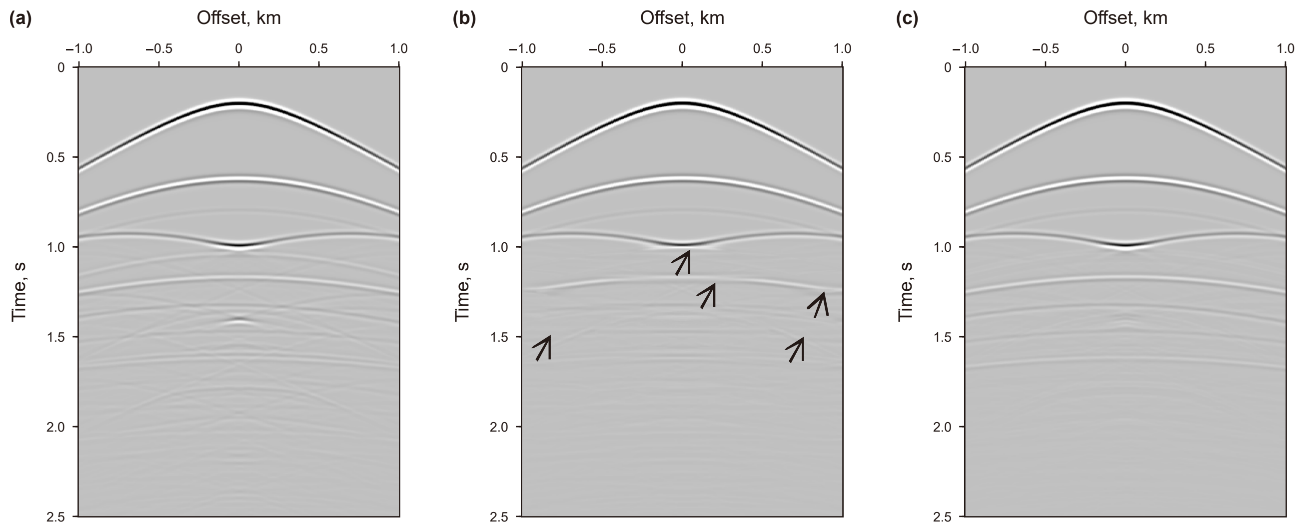

Fig. 13. Comparison of internal multiple suppression results. **(a)** Seismic record, **(b)** suppression result using IME, **(c)** suppression result using CL-IME.

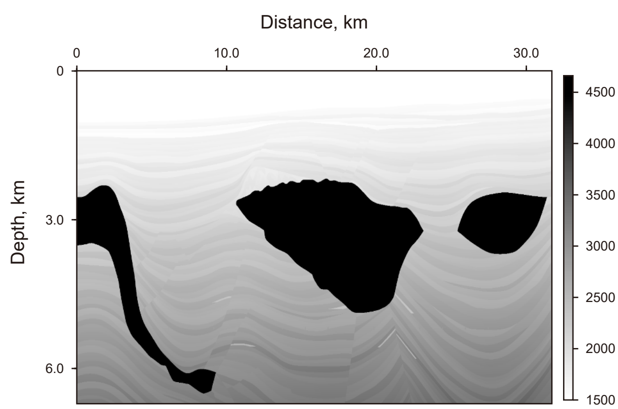

Fig. 14. SMAART JV Pluto model.

is achieved by directly subtracting them from the shot records (Fig. 4(d)), with the internal multiples accurately removed while primaries well preserved. Overall, the proposed CL-IME demonstrates a significant advantage in internal multiple suppression, particularly in complex regions where internal multiples overlap with primaries, outperforming the IME and validating its effectiveness and advantages.

To provide a clearer comparison of the two methods in terms of primary energy preservation, the overlapping region from Fig. 4(b) and (d) are extracted, and the corresponding waveforms are shown in Fig. 5. In this region, the suppression result of IME (Fig. 5(a)) exhibits evident weakening of primary energy, particularly at near-offset positions where the loss is more pronounced. In contrast, the CL-IME result (Fig. 5(b)) preserves the primary waveforms well, with a more uniform energy distribution, indicating that primary energy loss is effectively avoided

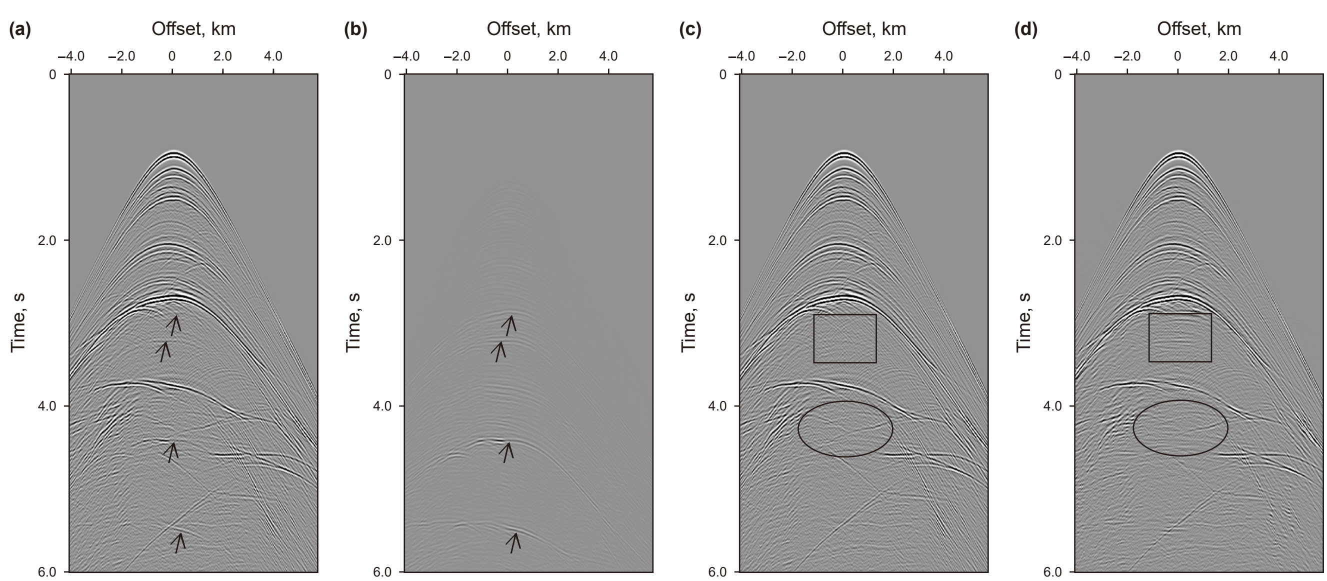

Fig. 15. Comparison of internal multiple suppression results. **(a)** Seismic record after removing surface-related multiples, **(b)** estimated internal multiples using CL-IME, **(c)** suppression result of internal multiples using CL-IME, **(d)** suppression result of internal multiples using IME.

during internal multiple suppression. These results further highlight the significant advantages of CL-IME in both the accuracy of internal multiple suppression and the preservation of primary amplitudes.

To provide a more intuitive comparison of the suppression performance of the two methods, the 80th trace is extracted from Figs. 3(b), 4(b) and (d). The waveforms within 0.8–1.36 s are compared with the corresponding ideal primaries, as shown in Fig. 6. It can be observed that significant energy interference between primaries and internal multiples exits within 1.23–1.28 s. Within this time window, both methods achieve suppression of internal multiples, but their suppression performance differs significantly. Compared with the primaries, the IME result exhibits noticeable amplitude loss, with an mean squared error (MSE) of 0.3350, indicating a relatively large deviation and substantial primary energy damage caused by the adaptive subtraction. In contrast, the CL-IME result closely matches the ideal primaries, with an MSE of 0.0528, which is significantly lower than that of the IME, demonstrating that the inversion strategy effectively preserves primary energy. These results indicate that the proposed CL-IME method exhibits a clear advantage in amplitude preservation.

To investigate the convergence characteristics of the proposed CL-IME method in the iterative inversion process, Fig. 7 shows its convergence curve. During the initial iterations, the residual exhibits a rapid decrease, indicating that the CL-IME method effectively reduces the data misfit within a limited number of iterations and demonstrates favorable convergence efficiency. With increasing iterations, the rate of residual reduction gradually diminishes and stabilizes after approximately ten iterations, exhibiting only minor fluctuations, indicating that the inversion process reaches a stable convergence regime. These observations indicate that the developed iterative inversion framework achieves stable convergence within a finite number of iterations while preserving the accuracy of internal multiple elimination, thereby confirming the robust convergence and numerical stability of the proposed CL-IME method.

To further investigate its adaptability and robustness under noisy conditions, additional analyses are conducted using noisy data, and the corresponding results are shown in Fig. 8. The seismic record with noise is shown in Fig. 8(a). The CL-IME is applied to suppress the internal multiples, and the estimated internal multiples are presented in Fig. 8(b), which closely match the internal multiples estimated from the noise-free data in Fig. 4(c). Fig. 8(c) illustrates the difference between the estimated multiples under noisy (Fig. 8(b)) and noise-free (Fig. 4(c)) conditions, where the discrepancies are barely noticeable, indicating that the influence of noise on the internal multiple estimation is limited. In the suppression result (Fig. 8(d)), the internal multiples are effectively suppressed while the primary energy in the interference region is well preserved, further demonstrating the robustness and adaptability of the proposed method in noisy conditions.

3.2. Complex model

To evaluate the adaptability of the proposed CI-IME under complex geological conditions, seismic data generated from a complex model (Fig. 9(a)) are used. A total of 201 sources are evenly distributed along the surface at 10 m intervals, with 201 detectors placed at the same spacing. The recording time is 2.5 s with a sampling interval of 4 ms. An absorbing boundary condition is applied, and the shot records can still be denoted as $\{\mathbf{P}\}_0$. An example of a single shot is shown in Fig. 9(b). The analysis indicates that the internal multiples are mainly related to the first and second boundaries ($\Delta\mathbf{M}_1$ and $\Delta\mathbf{M}_2$). Therefore, the CL-IME method is applied to suppress the internal multiples related to these two boundaries.

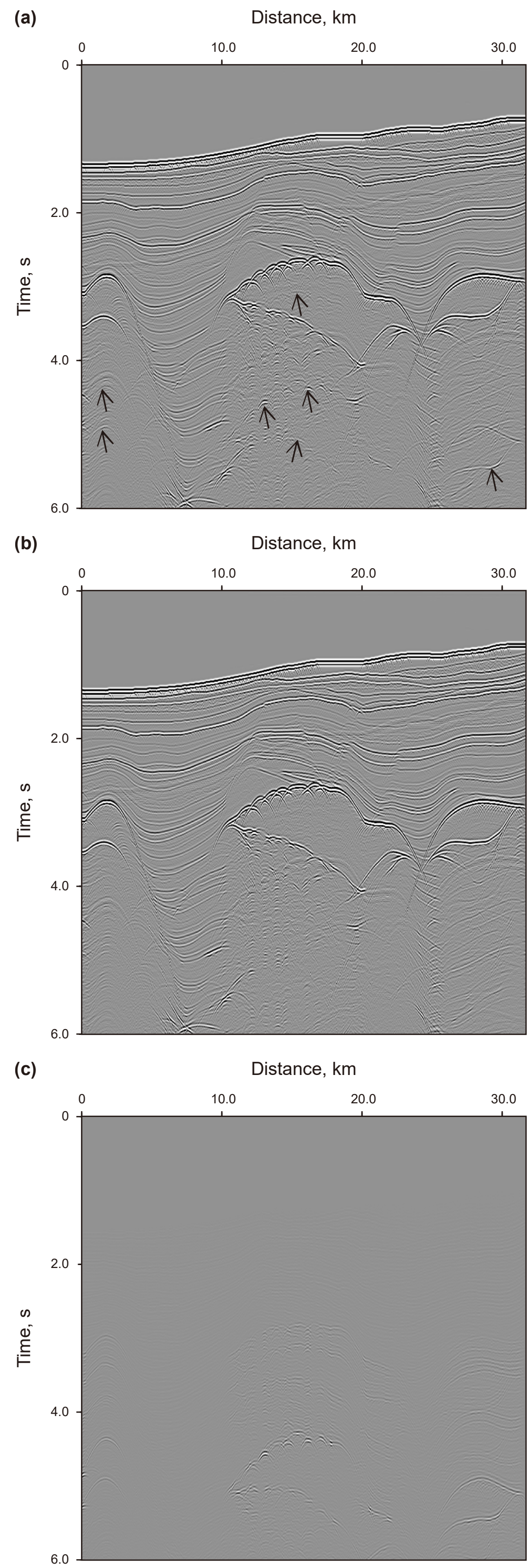

Fig. 16. Comparison of zero-offset sections. **(a)** Zero-offset section before internal multiple suppression, **(b)** zero-offset section after internal multiple suppression, **(c)** zero-offset section of the suppressed internal multiples.

First, the CL-IME method is applied to suppress the internal multiples $\Delta\mathbf{M}_1$, and the corresponding results are shown in Fig. 10. The shot records (Fig. 10(a)) clearly display internal multiples $\Delta\mathbf{M}_1$ (black arrows). After applying CL-IME, the estimated multiples (Fig. 10(b)) closely match the characteristics of the observed records, indicating the high accuracy of the internal multiple estimation. By directly subtracting these estimates from the shot records, the suppression result in Fig. 10(c) demonstrates that the internal multiples $\Delta\mathbf{M}_1$ are effectively suppressed, while the primary energy is well preserved without noticeable loss, verifying the effectiveness of the proposed CL-IME method.

Next, we further analyze the suppression results of internal multiples related to the subsequent boundary. As shown in the suppression result (Fig. 11(a)), internal multiples related to next boundary z_2 remain observable (black arrows). To address this, CL-IME is further applied to suppress the internal multiples $\Delta\mathbf{M}_2$, and the results are shown in Fig. 11. As seen in Fig. 11(b), CL-IME successfully estimates the internal multiples $\Delta\mathbf{M}_2$, with their shape, energy distribution, and spatial positions closely matching those in Fig. 11(a), demonstrating the accuracy of internal multiple estimation. Subtracting the estimated internal multiples $\Delta\mathbf{M}_2$ from Fig. 11(a) yields the final result as shown in Fig. 11(c), in which the multiple energy is effectively suppressed while the primary energy are well preserved. These results further confirm the adaptability and robustness of CL-IME under complex structural conditions.

To further evaluate the performance of CL-IME in the internal multiple suppression, zero-offset sections are extracted for comparison, as shown in Fig. 12. Fig. 12(a) is extracted from the seismic records, Fig. 12(b) is the suppression result of the internal multiples $\Delta\mathbf{M}_1$, and the final result after all internal multiples are removed is displayed in Fig. 12(c). In Fig. 12(a), internal multiples related to the top two boundaries can be clearly observed: $\Delta\mathbf{M}_1$ (black arrows) and $\Delta\mathbf{M}_2$ (white arrows). In Fig. 12(b), the internal multiples $\Delta\mathbf{M}_1$ is successfully suppressed, whereas the internal multiples $\Delta\mathbf{M}_2$ remain (white arrows). After further applying the CL-IME method to suppress the internal multiples $\Delta\mathbf{M}_2$, Fig. 12(c) shows that internal multiples $\Delta\mathbf{M}_2$ are effectively eliminated, while the primary energy is well preserved. These results clearly demonstrate the effectiveness and adaptability of CL-IME for layer-by-layer suppression of internal multiples.

To further evaluate the superiority of the proposed CL-IME under complex geological conditions, the suppression results of IME and CL-IME are compared in Fig. 13. As shown in the shot record (Fig. 13(a)), significant overlaps between primaries and internal multiples can be clearly observed at various locations. In Fig. 13(b), although IME suppresses internal multiple to some extent, its reliance on adaptive subtraction leads to noticeable primary energy loss. In contrast, CL-IME adopts an inversion-based strategy that avoids adaptive subtraction, thereby not only effectively suppressing internal multiples but also better preserving primary energy in overlapping regions (Fig. 13(c)). This comparison confirms the strong adaptability of CL-IME under complex conditions. Compared with IME, the proposed CL-IME provides more accurate suppression of internal multiples and superior amplitude preservation of primaries, thereby offering a more reliable data basis for subsequent seismic data processing.

3.3. SMAART JV Pluto

Next, the proposed CL-IME is applied to the SMAART JV Pluto (Fig. 14) dataset, which is publicly released by the Subsalt Multiples Attenuation and Reduction Technology Joint Venture. After suppressing the surface-related multiples, CL-IME is further employed to suppress the internal multiples.

The suppression results for a single shot are shown in Fig. 15. In Fig. 15(a), the internal multiples are indicated by black arrows. Through the inversion process in CL-IME, the internal multiples are accurately estimated (Fig. 15(b)). Since the estimated internal multiples closely match the original data in terms of shape, energy distribution, and spatial location, a simple subtraction is sufficient to remove the internal multiples from the shot records, yielding the final suppression result (Fig. 15(c)). As shown in Fig. 15(c), the internal multiples are effectively suppressed. Compared with the suppression result of the IME method (Fig. 15(d)), the CL-IME method achieves higher suppression accuracy (as indicated by the boxed region), while the primary energy is well preserved (as shown in the elliptical region).

Considering that internal multiples often exhibit kinematic characteristics similar to those of primaries, the zero-offset sections before and after suppression, together with the zero-offset section of the suppressed internal multiples, are extracted for analysis, as shown in Fig. 16. Because the strata above the high-velocity bodies (2.0–4.0 s) are nearly layered, the internal multiples in the zero-offset section display waveforms that closely resemble those of the primaries generated by the high-velocity bodies. Based on travel-time analysis, the main internal multiple energy can be identified in Fig. 16(a) (black arrows), and these multiples are

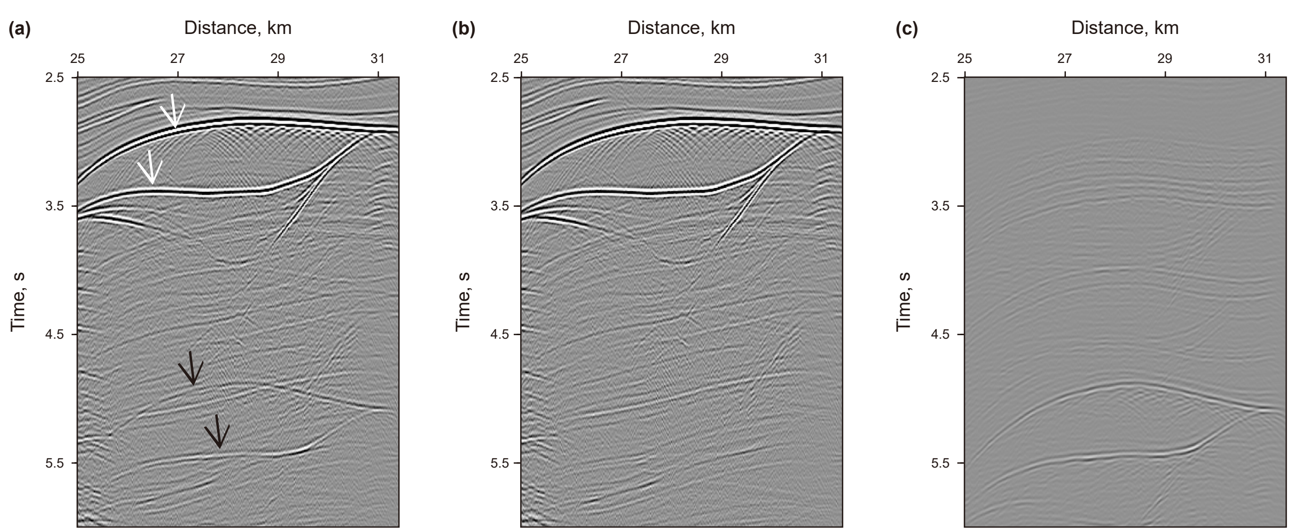

Fig. 17. Local enlargement of the zero-offset sections. **(a)** A portion of Fig. 16(a), **(b)** a portion of Fig. 16(b), **(c)** a portion of Fig. 16(c).

successfully suppressed using CL-IME, as shown in Fig. 16(b). Moreover, the zero-offset section of the estimated internal multiples (Fig. 16(c)) shows their shape is similar to that of the primaries, with a spatial distribution highly consistent with the internal multiples in Fig. 16(a), further demonstrating that CL-IME achieves accurate estimation and suppression of internal multiples.

Fig. 17 provides a detailed comparison of locally enlarged zero-offset sections from Fig. 16. Within the 4.8–5.5 s time window in Fig. 17(a), a set of events (black arrows) can be clearly observed, which are similar to the primaries generated from the high-velocity body at 2.5–3.5 s (white arrows), and exhibit the characteristics of internal multiples. In Fig. 17(b), the energy of the internal multiples is significantly attenuated compared with Fig. 17(a), while the primaries remain well preserved. Fig. 17(c) shows the estimated internal multiples, which are consistent with those in Fig. 17(a), further confirming the accuracy of the internal multiple estimation. This comparison demonstrates that CL-IME can effectively estimate and suppress internal multiples while preserving primary energy, thereby enhancing the overall quality of the section.

4. Conclusions

Based on the WRW model, a novel and solid mathematical and physical framework is established for internal multiple suppression under the feedback model. Within this framework, the subsurface boundary operator, which links the predicted multiples to actual multiples, depends solely on the reflection characteristics of the boundaries under certain assumptions, representing a novel and important finding that distinguished it from conventional methods.

However, similar to conventional methods, this method suffers from primary energy loss when primaries overlap with internal multiples due to its reliance on adaptive subtraction. To address this limitation, an inversion-based Closed-Loop Internal Multiple Elimination (CL-IME) method is proposed. By formulating an objective function and performing inversion, internal multiples can be accurately estimated and removed from seismic data, effectively avoiding the primary energy loss caused by adaptive subtraction. Numerical results demonstrate that the proposed CL-IME not only achieves significantly higher accuracy in internal multiple suppression but also preserves primary amplitudes in regions where primaries and internal multiples overlap, thereby providing a more reliable foundation for subsequent seismic data processing. While the incorporation of inversion improves suppression accuracy, it also leads to increased computational cost. Therefore, enhancing the computational efficiency of the method represents an important direction for future research.

CRediT authorship contribution statement

Zi-Lin He: Writing – original draft, Visualization, Validation, Methodology. **Zhi-Na Li:** Writing – review & editing, Project administration, Conceptualization. **Zhen-Chun Li:** Supervision, Resources, Funding acquisition. **Yi-Peng Xu:** Investigation, Data curation. **Yan-Yun Leng:** Investigation, Formal analysis.

Declaration of competing interest

The authors declare that they have no known competing financial interests or personal relationships that could have appeared to influence the work reported in this paper.

Acknowledgments

This work is supported the National Natural Science Foundation of China under Grant Nos. 42574163 and 42574164, Fund of State Key Laboratory of Deep Oil and Gas under Grant No. SKLDOG2024-ZYTS-05, Qingdao Natural Science Foundation under Grant No. 24-4-4-zrjj-186-jch, Young Talent of Lifting engineering for Science and Technology in Shandong under Grant No. SDAST2025 QTB055, Dongying Natural Science Foundation under Grant No. 2025ZR027 and Natural Science Foundation of Shandong Province under Grant No. ZR2025QC452.

References

Araújo, F.V., Weglein, A.B., Carvalho, P.M., et al., 1994. Inverse scattering series for multiple attenuation: An example with surface and internal multiples. SEG Technical Program Expanded Abstracts 1994, pp. 1039–1041. https://doi.org/10.1190/1.1822691.

Bao, P.N., Shi, Y., Wang, W.H., et al., 2022. An improved method for internal multiple elimination using the theory of virtual events. Pet. Sci. 19 (6), 2663–2674. https://doi.org/10.1016/j.petsci.2022.05.021.

Berkhout, A.J., 1982. In: Seismic Migration, Imaging of Acoustic Energy by Wave Field Extrapolation: Theoretical Aspects, second ed. Elsevier Science Publishing Co., Inc., Amsterdam.

Berkhout, A.J., 1997. Pushing the limits of seismic imaging—Part I: prestack migration in terms of double dynamic focusing. Geophysics 62 (3), 937–953. https://doi.org/10.1190/1.1444201.

Berkhout, A.J., 1999. Multiple removal based on the feedback model. Lead. Edge 18 (1), 127–131. https://doi.org/10.1190/1.1438140.

Berkhout, A.J., Verschuur, D.J., 1997. Estimation of multiple scattering by iterative inversion, part 1: theoretical considerations. Geophysics 62 (5), 1586–1595. https://doi.org/10.1190/1.1887382.

Berkhout, A.J., Verschuur, D.J., 2005. Removal of internal multiples with the common-focus-point (CFP) approach: part 1—Explanation of the theory. Geophysics 70 (3), V45–V60. https://doi.org/10.1190/1.1925753.

Berkhout, A.J., Verschuur, D.J., 2012. Full wavefield migration – Utilization of multiples in seismic migration. In: 74th EAGE Conference and Exhibition Incorporating EUROPEC 2012. https://doi.org/10.3997/2214-4609.20148155.

Gong, S., Ren, Q.Q., Wang, M.L., 2017. Application of parabolic radon transform in the suppression of multiple seismic wave. CT Theor. Appl. 26 (2), 165–176. https://doi.org/10.15953/j.1004-4140.2017.26.02.05 (in Chinese).

Groenestijn, G.J.A.V., Verschuur, D.J., 2009. Estimation of primaries and near-offset reconstruction by sparse inversion: marine data applications. Geophysics 74 (6), R119–R128. https://doi.org/10.1190/1.3213532.

Gu, Z., Geng, J., Wu, R.S., 2023. An application of internal multiple prediction and primary reflection retrieval to salt structures. Geophysics 88 (6), S189–S201. https://doi.org/10.1190/geo2022-0669.1.

Hung, B., Wang, M., 2012. Internal demultiple methodology without identifying the multiple generators. SEG Technical Program Expanded Abstracts 2012 segam2012-0549.1. https://doi.org/10.1190/segam2012-0549.1.

Ikelle, L.T., 2006. A construct of internal multiples from surface data only: The concept of virtual seismic events. Geophys. J. Int. 164 (2), 383–393. https://doi.org/10.1111/j.1365-246X.2006.02857.x.

Jakubowicz, H., 1998. Wave equation prediction and removal of interbed multiples. In: 60th EAGE Conference and Exhibition, cp-110-00074. https://doi.org/10.3997/2214-4609.201408173.

Li, C., Liu, G., Chen, X., et al., 2024. Joint reconstruction and multiple attenuation using one-step randomized-order damped rank reduction method. IEEE Trans. Geosci. Rem. Sens. 62, 5921611. https://doi.org/10.1109/TGRS.2024.3435560.

Santos, R.S., Revelo, D.E., Pestana, R.C., et al., 2021. An application of the Marchenko internal multiple elimination scheme formulated as a least-squares problem. Geophysics 86 (5), WC105–WC116. https://doi.org/10.1190/geo2020-0825.1.

Thorbecke, J.W., 1997. Common Focus Point Technology. Ph.D. Thesis, Delft University of Technology, Delft, Nederland.

van Borselen, R., 2002. Data-driven interbed multiple removal: Strategies and examples. In: SEG Technical Program Expanded Abstracts 2002, pp. 2106–2109. https://doi.org/10.1190/1.1817119.

Yang, J.L., Zhu, L.H., 2018. Inverse scattering series internal multiple attenuation method and its application. Geophys. Prospect. Pet. 57 (6), 853–861. https://doi.org/10.3969/j.issn.1000-1441.2018.06.007 (in Chinese).

You, J.C., Zhang, G.L., Huang, X.G., et al., 2025. Internal-multiple-elimination with application to migration using two-way wave equation depth-extrapolation scheme. Pet. Sci. 22 (1), 178–192. https://doi.org/10.1016/j.petsci.2024.06.021.

You, J.C., Cao, J.X., 2020. Full wave equation depth extrapolation for migration using matrix multiplication. Geophysics 85 (6), S395–S403. https://doi.org/10.1190/geo2019-0323.1.

Ypma, F.H.C., Verschuur, D.J., 2013. Estimating primaries by sparse inversion, a generalized approach. Geophys. Prospect. 61 (s1), 94–108. https://doi.org/10.1111/j.1365-2478.2012.01095.x.

Zhang, L.L., Thorbecke, J., Wapenaar, K., et al., 2019. Transmission compensated primary reflection retrieval in the data domain and consequences for imaging. Geophysics 84 (4), Q27–Q36. https://doi.org/10.1190/geo2018-0340.1.

Zhang, L.L., Staring, M., 2018. Marchenko scheme based internal multiple reflection elimination in acoustic wavefield. J. Appl. Geophys. 159, 429–433. https://doi.org/10.1016/j.jappgeo.2018.09.024.